scientific reports

Check for updates

OPEN

# Poly(bromophenol blue)/ $CoSn(OH)_6$ cubic particles modified pencil graphite electrode for electrochemical determination of diphenhydramine

Serkan Karakaya[1✉], Sezgin Bakırdere[2,3], Meltem Şaylan[2,4] & Yusuf Dilgin[1]

**In this study, a poly(bromophenol blue) (poly(BPB))-coated $CoSn(OH)_6$ cubic particles -modified pencil graphite electrode (poly(BPB)@$CoSn(OH)_6$/PGE) was developed, and its electrochemical activity towards diphenhydramine (DPHN) oxidation was systematically investigated. Cyclic voltammetric studies revealed that the oxidation of DPHN at the modified electrode is governed by a diffusion-controlled process, indicating strong interaction between DPHN molecules and the poly(BPB) film. The incorporation of the $CoSn(OH)_6$ cubic structure enhances electron transfer kinetics by increasing the density of electroactive sites and facilitating charge transport across the electrode interface. This cooperative interaction between the conductive polymer and metal hydroxide structure results in a significant amplification of the oxidation response. Under optimized conditions, the proposed electrode exhibited a linear response in the concentration range of 1.0–500.0 µM with a detection limit (LOD) of 0.30 µM. Although the analytical performance is comparable to previously reported systems, the present work provides deeper insight into the role of polymer–metal hydroxide interfaces in governing electrochemical sensing behavior. The sensor also demonstrated acceptable selectivity and applicability in pharmaceutical, biological, and environmental samples. These findings highlight the importance of interfacial design in improving electrochemical performance and offer a useful framework for developing advanced hybrid sensing platforms.**

**Keywords** Diphenhydramine, Bromophenol blue, $CoSn(OH)_6$ cubic particles, Pencil graphite electrode, Cyclic voltammetry, Electrochemical sensor

DPHN, chemically known as 2-(diphenylmethoxy)-N, N-dimethylethanamine, is a first-generation antihistaminic drug acting as an H1 receptor antagonist[1]. Owing to its long-standing clinical use, spanning over several decades, DPHN is widely administered for the treatment of allergic conditions, sleep disorders, and common cold symptoms across different age groups[2,3]. Despite its therapeutic benefits, the pharmacological and toxicological effects of DPHN are strongly dose-dependent. While low doses generally lead to mild symptoms, excessive intake may result in severe adverse effects such as delirium, seizures, rhabdomyolysis, coma, and even death[4]. Furthermore, its misuse and abuse potential have been increasingly reported due to its psychoactive effects, including mood alteration and hallucinations[5]. Therefore, the reliable determination and monitoring of DPHN in pharmaceutical, biological, and environmental samples are of significant importance for public health and drug safety[6].

Various analytical techniques have been employed for the determination of DPHN, including spectrophotometry[7,8], chromatography[9,10], titrimetry[11], and electrochemical methods[3,12–15]. Although chromatographic and spectroscopic approaches offer high sensitivity and accuracy, they are often associated with limitations such as expensive instrumentation, time-consuming sample preparation, and the need for skilled personnel[5,13]. In addition, these techniques are generally restricted to centralized laboratory settings, which

[1]Chemistry Department of Science Faculty, Çanakkale Onsekiz Mart University, 17020 Çanakkale, Turkey. [2]Chemistry Department of Yıldız, Technical University, 34220 İstanbul, Turkey. [3]Turkish Academy of Sciences (TÜBA), Çankaya, Vedat Dalokay Street, No. 112, 06670 Ankara, Turkey. [4]Department of Pharmacy, İstanbul Health and Technology University, 34421 İstanbul, Turkey. ✉email: skarakaya@comu.edu.tr

limit their applicability for rapid and on-site analysis. In this context, electrochemical methods have attracted increasing attention as alternative analytical tools due to their inherent advantages, including simplicity, rapid response, low cost, and suitability for miniaturization[16]. Among electrochemical approaches, voltammetric techniques have been extensively utilized for trace-level detection owing to their high sensitivity and operational convenience. However, the performance of electrochemical sensors is strongly dependent on the properties of the electrode surface. Unmodified electrodes often suffer from high overpotentials and poor sensitivity, which significantly limits their analytical applicability[6]. To overcome these limitations, various surface modification strategies involving conductive polymers[17], organic mediators[18], metal complexes[19], nanoparticles[20], and composite nanomaterials[21,22] have been developed. In particular, PGEs have emerged as attractive platforms due to their low cost, disposability, ease of modification, and favorable electrochemical properties compared to conventional carbon-based electrodes such as glassy carbon electrode (GCE) and carbon paste electrode (CPE)[23].

Conductive polymers have received considerable attention as electrode modifiers due to their tunable conductivity, strong adhesion to electrode surfaces, and ease of synthesis. Among the available fabrication methods, electropolymerization is especially advantageous as it enables precise control over film thickness, morphology, and electrochemical properties during the polymer growth process[6]. In recent years, electroactive polymers derived from organic dyes have gained prominence due to their redox activity and ability to mediate electron transfer processes. BPB, a triphenylmethane-based dye, is particularly attractive owing to its electrochemical reversibility, high electron transfer rate, and strong adsorption capability on electrode surfaces[24]. In addition, poly(BPB) is particularly outstanding as a redox-active polymer for electrode modification. Depositing poly(BPB) films onto the transducer surface creates robust pathways that accelerate charge transfer kinetics and boost current responses[24–26]. Beyond its intrinsic electroactivity, this polymeric backbone acts as an effective matrix to stabilize inorganic nanomaterials and improve overall sensor durability. These features make poly(BPB) a promising candidate for facilitating adsorption-driven electrochemical processes and enhancing interfacial charge transfer.

In addition to conductive polymers, transition metal hydroxide nanostructures have been widely explored as electrocatalytic materials due to their large surface area and rich active sites[27]. Among them, perovskite-like structured metal hydroxystannates ($MSn(OH)_6$) with $d^{10}$–$d^{10}$ configuration have attracted attention due to its unique three-dimensional architecture and tunable electronic properties. Various morphologies of $MSn(OH)_6$, such as cubic particles, nanospheres, and nanoboxes, have been reported and applied in energy storage and catalytic systems[28–32]. The presence of transition metal centers with partially filled d-orbitals contributes to enhanced electrocatalytic activity, while the incorporation of Sn-based components can improve conductivity when combined with suitable conductive materials[27]. Exhibiting excellent physical and chemical properties with its special cell structure, these perovskite types ($MSn(OH)_6$) mostly contain transition metals such as Co, Zn, and Cu as M. Due to their large specific surface area, diverse morphological structures, and high catalytic activity, they have been used in fields such as supercapacitor[33] and oxygen evolution reaction (OER) studies[34], gas sensors[35], and photocatalysts[36]. In addition, these materials have been used in the electrochemical determination of analytes such as rutin[27], tryptophan[37], acetaminophen[38], and $H_2O_2$[39] as they provide active sites that increase the affinity of analytes and provide good electrocatalytic activity. $MSn(OH)_6$ type perovskite materials are used as an preferable modification material in the electrode fabrication due to their ability to overcome problems caused by overpotential and increase electron transfer rate, thus significantly improving the electrocatalytic properties, stability, and reproducibility of bare electrodes[37].

Rapid and low-cost determination of antihistamines is important for both clinical monitoring and environmental pollution control. Thus in recent years a wide variety of modified electrodes have been developed for the electrochemical determination of DPHN. For example, $Gd_2ZnMnO_6$/ZnO/ionic liquid nanocomposite modified CPE[3], CuNPs/ poly(Alizarin Yellow R)/GCE[6], and CdO/single wall carbon nanotubes/1-butyl-3-methylimidazolium hexafluoro phosphate/CPE[15] have been successfully proposed for the sensitive determination of DPHN. However, the polymer-$CoSn(OH)_6$ composite modified electrode has not yet been used in the determination of antihistamines. As mentioned above, it is predicted that combining the conductivity and electron transfer-enhancing effect of the polymer with the large surface area properties offered by the cubic structures of $CoSn(OH)_6$ will exhibit a significant increase in the signal of the electrooxidation of DPHN. Consequently, in this study, a more sensitive and selective determination of DPHN was achieved by taking advantage of the synergy of the Poly(Bromophenol blue)/$CoSn(OH)_6$ hybrid structure.

In light of these considerations, the present study introduces a rationally designed electrochemical sensing platform that prioritizes simplicity, reproducibility, and practical usability without compromising analytical performance. The proposed system is based on the integration of an electropolymerized poly(BPB) film with $CoSn(OH)_6$ cubic particles on a PGE, enabling the formation of a stable and electroactive interface through a straightforward preparation route. Unlike many existing strategies that rely on structurally complex or resource-intensive materials, this approach exploits the complementary interaction between a redox-active polymer matrix and a perovskite-like hydroxide structure to facilitate efficient charge transfer and consistent signal generation. The resulting sensor demonstrates reliable performance across multiple sample environments, highlighting its adaptability beyond controlled laboratory conditions. From a broader perspective, this work contributes to the ongoing transition in electrochemical sensing research from sensitivity-driven designs toward application-oriented systems that can be realistically implemented in routine analysis. The conceptual framework presented here may inspire the development of next-generation sensors that combine low-cost electrode substrates with functional polymer–inorganic hybrids, offering scalable and versatile solutions for pharmaceutical monitoring and environmental analysis. Future studies may further expand this strategy by tailoring polymer structures or incorporating alternative metal-based structures to enhance selectivity and extend the applicability of such platforms to a wider range of target analytes.

## Experimental

### Materials and instrumentation

Diphenhydramine hydrochloride ($C_{17}H_{21}NO{\cdot}HCl$, 291.82 g $mol^{-1}$) was procured from TLC standards. All other chemicals used in this study were of analytical-grade purity and procured from the suppliers of Sigma-Aldrich, Thermo Scientific Chemicals, and Merck. A Compactstat-Interface device by Ivium Technologies (Netherlands) was utilized for all electrochemical experiments. All electrochemical data were collected using Ivium software. A Q7B series water-purification device from Elga Option with an 18.2 MΩ resistivity was used to receive the ultra-pure water for the preparation of Britton-Robinson buffer (B-RB) solutions. The pH arrangement of the buffers was performed with a Hanna 221 series apparatus coupled with a combined glass electrode. An $Ag/AgCl_{(3.0\ M\ KCl)}$ (reference electrode, BASI), a Pt wire (auxiliary electrode, BASI), and a working electrode of bare/modified PGE (TOMBOW 2B lead with a diameter of 0.50 mm) involved a three-electrode system in an electrochemical cell. A 1.0 cm length of PGE was used in all electrochemical measurements. A steel syringe needle with a diameter of 0.60 mm (GENJECT) was used as the holder of PGE, and the electrical connection was made by brazing a copper wire onto the steel part of the needle.

Techniques such as scanning electron microscopy (SEM), energy-dispersive X-ray (EDX) spectroscopy, X-ray diffraction (XRD), and Fourier-transform infrared (FT-IR) spectroscopy were utilized for the morphological and structural identification of the electrodes by using a JSM-7100-F series of JEOL scanning electron microscopy (SEM) device equipped with an EDX module, a PANalytical Empyrean XRD device, and a Spectrum 100 model FTIR spectrophotometer of Perkin Elmer equipped with a sampling accessory of attenuated total reflectance (ATR), respectively.

### Preparation of cubic structured $CoSn(OH)_6$

The $CoSn(OH)_6$ cubic particles were prepared according to a previously declared procedure[40]. For this aim, 1.0 mmol of $CoCl_2$ and 1.0 mmol of trisodium citrate ($Na_3C_6H_5O_7$) were dissolved in water. Then, 1.0 mmol of $SnCl_4$ was added to the mixed solution drop by drop. After the mixture solution was stirred for a while, the precipitation process was carried out by the addition of 2.0 M 5.0 mL NaOH solution and stirred for an additional half an hour. The color of the solution, which was purple as soon as the precipitation process started, turned to pink when the addition was completed, and pink-colored precipitates were observed. The suspension was kept in a cabinet away from light to allow the sediments to accumulate at the bottom of the flask and to facilitate separation. After that, the suspension was centrifuged, and the precipitate was washed with pure water to eliminate the impurities. Then, the precipitate was dried at 50–55 °C in a drying oven for 12 h to obtain $CoSn(OH)_6$ cubic particles.

### Preparation of the poly(BPB)@$CoSn(OH)_6$/PGE

The $CoSn(OH)_6$/PGE was prepared by immersing the bare PGE into an ethanol (EtOH) suspension including 2.0 mg $mL^{-1}$ of $CoSn(OH)_6$ for 90 s. Then, the resulting $CoSn(OH)_6$/PGE was coated with redox-active BPB polymer film by recording the cyclic voltammograms (CVs) of the monomer solution containing 0.30 mM BPB + 0.10 M NaOH + 0.10 M KCl (The range of applied potential (RAP): -0.20 V – +1.80 V, sweep rate ($\nu$): 100 mV $s^{-1}$, and number of cycles: 3). The prepared poly(BPB)@$CoSn(OH)_6$/PGE was dried at room temperature before use. The fabrication process of the DPHN sensing platform is also schematically demonstrated in Fig. 1. The optimizations of some parameters such as immersing time of pencil leads into 2.0 mg $mL^{-1}$ of $CoSn(OH)_6$, BPB concentration, and cycle number during the preparation of the composite electrode were examined based on peak current obtained from the CVs of 0.50 mM DPHN for each parameter. The optimal conditions based on the highest oxidation peak current of DPHN were determined as 90 s, 0.30 mM, and 3 cycles, in order.

### Procedure for real sample analysis

The pharmaceutical formulation (KALMOSAN lotion cream, containing 1.0% (w/w) diphenhydramine hydrochloride) was purchased from a pharmacy. The tap water was collected from Çanakkale city in Türkiye. A published procedure was used for the preparation of the artificial human blood serum[41]. The standard addition and recovery protocols were used for DPHN analysis in the mentioned real samples. Firstly, the cream was diluted with B-RB solution (pH 10.0) in an electrochemical cell (dilution ratio is 1:1374 which approximately equals to 25 µM predicted DPHN concentration), and the CVs of the resulting solution were recorded under optimal conditions. Then, the appropriate standard additions were made from the stock DPHN solution, and the CVs were similarly recorded. The standard addition-calibration graph was drawn for the calculation of the DPHN content of the cream sample.

The validation of the proposed method was performed by a published Ultraviolet-Visible (UV-Vis) spectrophotometric procedure with a small modification[42]. According to the procedure mentioned, the 25 mL of DPHN standards (2.0, 4.0, 6.0, 8.0, and 10 µg $mL^{-1}$) were prepared by appropriate dilutions from a 200 µg $mL^{-1}$ stock DPHN solution prepared in EtOH. Then, 1.0 M NaOH (1.0 mL) and 0.2% $KMnO_4$ (1.0 mL) were added to each solution and sonicated for 15 min. Then, the water was added until reaching the final volume. The absorbance value of each standard was recorded at 610 nm of wavelength to generate a calibration graph based on absorbance versus DPHN concentration. The same procedure was followed for the lotion sample, and the appropriate dilution was made to ensure the DPHN concentration reached the relevant calibration range, and the absorbance was recorded. Finally, the DPHN content of the sample was calculated using the calibration graph.

To evaluate the method's accuracy and matrix effects, a recovery study was conducted using the standard addition technique. The pharmaceutical sample was spiked with known concentrations of DPHN (0.5% and 1.0%). The measurements were performed in triplicate ($n = 3$) to ensure statistical reliability. For comparison, the same samples were analyzed using the proposed UV-Vis spectrophotometric method as the reference. The

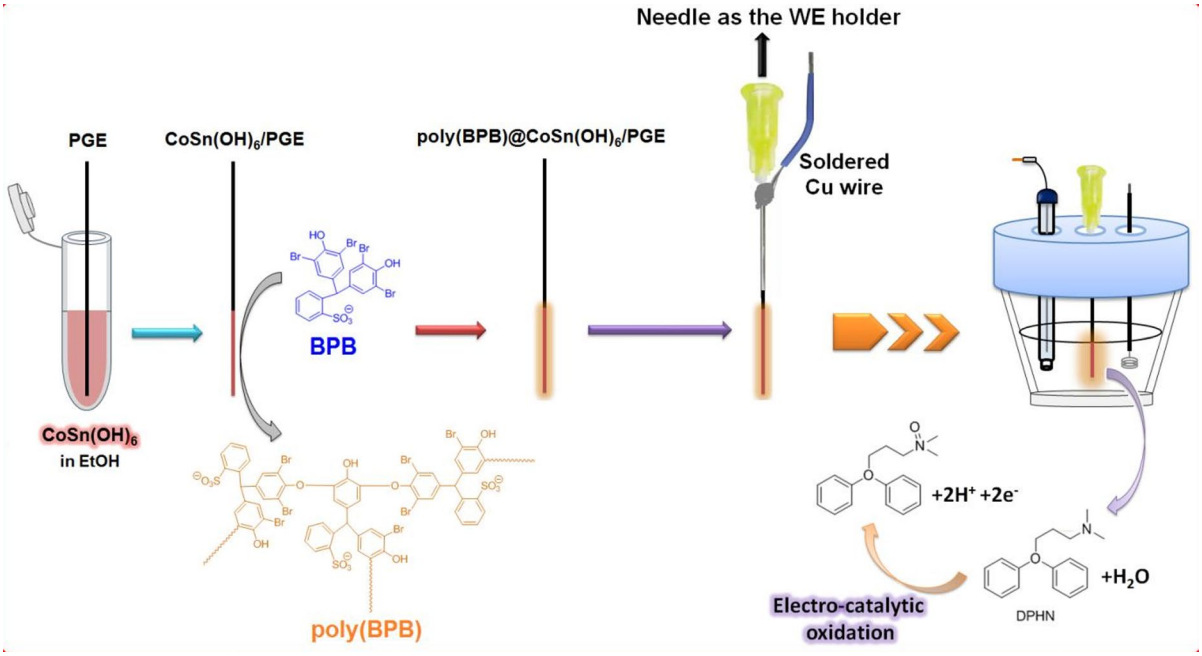



**Fig. 1**. The schematic demonstration for the fabrication of poly(BPB)@CoSn(OH)$_6$/PGE.

recovery percentages were calculated by comparing the measured values against the known spiked concentrations to determine the method's accuracy and potential interference from the lotion matrix.

The determination of the DPHN in natural spring water and the artificial human blood serum was also utilized by monitoring the CVs of two different spiked amounts (25 and 50 µM) of DPHN under optimized conditions. Then, the standard additions were performed, and the CVs were similarly recorded for each addition. The recovery percentages were calculated for each sample.

## Result and discussion

### The characterization of CoSn(OH)$_6$ cubic particles

The characterization profiles illustrated in Fig. 2 are systematically arranged to follow the real-time synthesis and surface modification sequence. Following the primary phase verification of the CoSn(OH)$_6$ core via XRD (Fig. S1A), the dynamic interfacial growth of the polymeric matrix was monitored (Fig. S1B), which was subsequently validated through structural functional group variations via ATR-FTIR analysis (Fig. S1C). CoSn(OH)$_6$ cubic particles were characterized by the XRD technique. The XRD pattern of CoSn(OH)$_6$, in the 2-theta range of 10–90°, was given in Fig. S1A. Sharp and strong diffraction peaks were observed at 2-theta values of 19.844°, 22.971°, 32.668°, 36.720°, 38.610°, 40.334°, 46.914°, 51.390°, 52.832°, 58.254°, 68.530°, 72.200°, 73.170°, 77.890°, 82.410°, and 86.958° which are related to the planes of (111), (200), (220), (310), (311), (222), (400), (331), (420), (422), (440), (531), (442), (620), (622), and (444) in order. It has been revealed that CoSn(OH)$_6$ cubic particles with octahedral coordination structure and cubic crystal structure have been synthesized and found to be compatible with the literature[33,35,43–45].

### The fabrication and characteristics of poly(BPB)@CoSn(OH)$_6$/PGE

The electropolymerization of BPB at CoSn(OH)$_6$/PGE was utilized in the monomer solution containing 0.30 mM BPB + 0.10 M NaOH + 0.10 M KCl (RAP: − 0.20 V - +1.80 V, $\nu$ = 100 mV s$^{-1}$, and number of cycles: 3). Fig. S1B illustrates the typical set of CVs achieved from the electropolymerization of BPB on the CoSn(OH)$_6$/PGE. A broad oxidative peak at + 1.60 V in the 1st cycle shifted to + 1.55 V in the 2$^{nd}$ with an increment in peak current, and a new peak was observed at + 1.15 V, and the current of this peak also increased in the 3$^{rd}$ cycle. The shift in anodic current ($I_p$) and the observation of a new oxidation peak are acceptable evidence for the formation of BPB polymer film at CoSn(OH)$_6$/PGE. Moreover, a possible mechanism for BPB electropolymerization was given in Fig. S2. The phenoxy radical of BPB occurred by the separation of $2H^+$ and $2e^-$ due to the electrochemical oxidation step (I), and an intermediate product, a quinoid structure, formed (II). After the nucleophilic attack of the negatively charged oxygen ion on the bromine-bonded aromatic carbon atom, the bromine ion divorced from the quinoid intermediate to give a dimer structure (III), by further coupling and electrochemical reduction processes (IV-VII) to build up the poly(BPB) network. As reflected in the scheme, there are many active positions for the prolongation of the polymeric chain, so the polymer structure can be formed[46].

The ATR-FTIR spectra of monomer BPB and poly(BPB) were recorded to obtain advanced evidence for the formation of the polymer film (Fig. S1C). For this characterization, electropolymeric deposition was performed on GCE, which is more suitable for recording FTIR spectra on ATR, and is mechanically more resistant and convenient during pressing, instead of PGE. The characteristic stretching vibration bands at 3471 cm$^{-1}$ (-O-H),

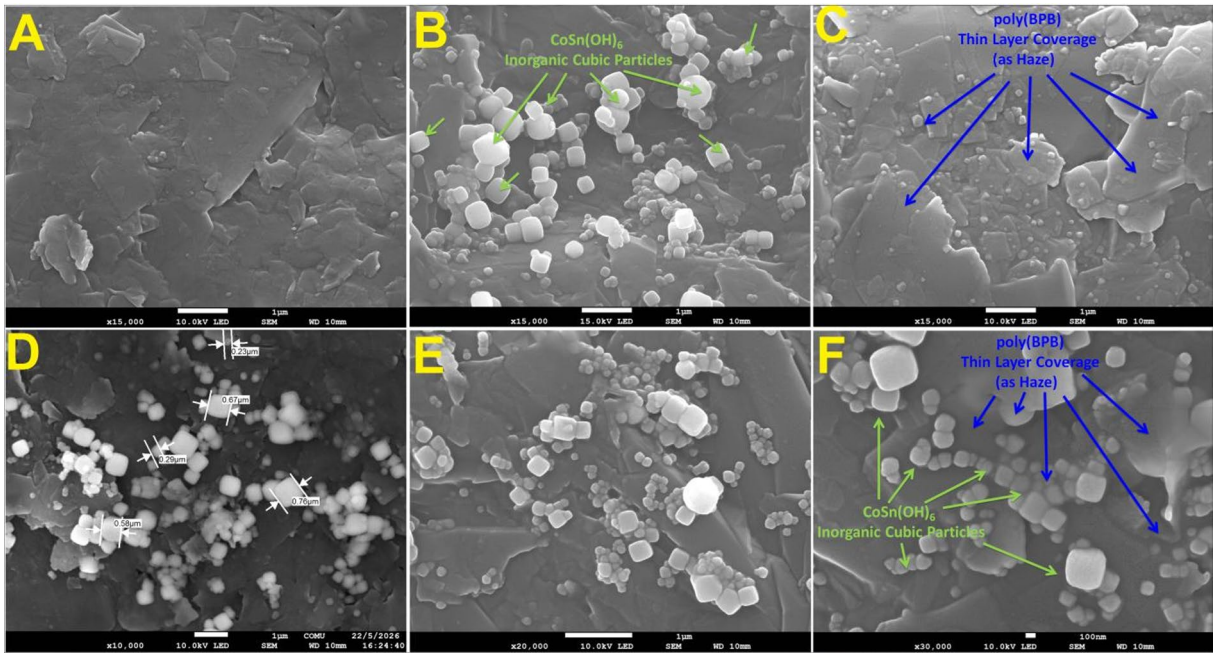



**Fig. 2**. SEM micrographs for (**A**) unmodified PGE (1.0 μm ×15000), (**B**) $CoSn(OH)_6$/PGE (1.0 μm ×15000), (**C**) poly(BPB)@PGE (1.0 μm ×15000), (**D**) poly(BPB)@$CoSn(OH)_6$/PGE (1.0 μm ×15000), and increased magnifications of SEM images for poly(BPB)@$CoSn(OH)_6$/PGE (**E**) (1.0 μm ×20000) and (**F**) (100 nm ×30000).

1473 $cm^{-1}$ (aliphatic -C-H), 1346 $cm^{-1}$ (asymmetric S=O stretching of $-SO_3$), 1189 $cm^{-1}$ and 1158 $cm^{-1}$ (symmetric S=O stretching of $-SO_3$), and 751 $cm^{-1}$ (C–Br stretching) can be easily seen in the FT-IR spectrum of BPB monomer (curve a). After electropolymerization of BPB, the vibration bands observed at 3306 $cm^{-1}$ (H-bond interaction), 1641 $cm^{-1}$ and 1551 $cm^{-1}$ (C=C stretchings of substitute biphenyl groups), 1201 $cm^{-1}$ (asymmetric phenolic ether, C–O–C stretching), and 1079 $cm^{-1}$ (symmetric phenolic ether, C–O–C stretching) confirm the formation of polymeric BPB film on the surface (curve b). All the changes in FT-IR spectra clearly affirm the successful formation of the poly(BPB) network by the proposed polymerization technique[46].

The electrochemical characteristics of all electrodes were examined by monitoring the CVs (Fig. S1D) and electrochemical impedance spectroscopy (EIS) curves (Fig. S1E) of 5.0 mM $Fe(CN)_6^{3-/4-}$ +0.10 M KCl solution. The reduction and oxidation peaks of the $Fe(CN)_6^{3-/4-}$ redox probe at bare PGE (curve a) increase with the individual modifications of poly(BPB) (curve b) and $CoSn(OH)_6$ (curve c) at PGE, due to the superior electrical, structural, and electrochemical properties of these materials as explained in the introduction section. Moreover, a notable improvement was observed in the related peaks after the dual modification of poly(BPB) and $CoSn(OH)_6$ at PGE (curve d). Additionally, EIS experiments were utilized to validate the results of CV measurements. Fig. S1D shows the EIS curves of bare PGE (curve a), poly(BPB)@PGE (curve b), $CoSn(OH)_6$/PGE (curve c), and poly(BPB)@$CoSn(OH)_6$/PGE (curve d). The inset of Fig. S1E indicates the fitted experimental data based on the Randles equivalent circuit model, which explained the ohmic (solution) resistance ($R_s$), charge transfer resistance ($R_{ct}$), Warburg impedance (W), constant phase element (C), and working electrode (WE). As can be understood from the EIS (Fig. S1E), $R_{ct}$ values were measured as 113, 93, 77, and 39 Ω for PGE, poly(BPB)@PGE, $CoSn(OH)_6$/PGE, and poly(BPB)@$CoSn(OH)_6$/PGE, respectively. Thus, these $R_{ct}$ results were found to be in good agreement with peak current increments from the CV data and confirmed the high conductivity and availability of poly(BPB)@$CoSn(OH)_6$/PGE in utilization of electrochemical sensing.

The effective surface areas ($A_{Eff}$ as $cm^2$) for the electrodes were determined according to the equation of Randles-Sevcik (Eq. 1)[17]. The $I_p$, the number of electrons ($n = 1$), the concentration of $Fe(CN)_6^{3-/4-}$ redox probe ($C = 5.0 \times 10^{-6}$ mol/$cm^3$), and the diffusion coefficient ($D = 6.23 \times 10^{-6}$ $cm^2/s$)[17] of the $Fe(CN)_6^{3-/4-}$ solution were taken into consideration, and the $A_{Eff}$ values were found as 0.200, 0.239, 0.250, and 0.301 $cm^2$ for bare PGE, poly(BPB)@PGE, $CoSn(OH)_6$/PGE, and poly(BPB)@$CoSn(OH)_6$/PGE, respectively. The significant improvement in $A_{Eff}$ value (0.301 $cm^2$) at poly(BPB)@$CoSn(OH)_6$/PGE highlights that the incorporation of the poly(BPB)@$CoSn(OH)_6$ composite material significantly enhances the number of electroactive sites on the PGE surface by the interaction between the poly(BPB) and $CoSn(OH)_6$. This interaction significantly upgrades the composite's efficiency and stability, turning poly(BPB)@$CoSn(OH)_6$ into a suitable choice for high-performance sensor applications such as DPHN monitoring.

$$I_p = 2.69 \times 10^5 \times n^{3/2} \times A_{Eff} \times C \times D^{1/2} \times v^{1/2} \quad (1)$$

The surface morphologies of bare PGE, poly(BPB)@PGE, $CoSn(OH)_6$/PGE, and poly(BPB)@$CoSn(OH)_6$/PGE were investigated using acquired SEM images (Fig. 2) and EDX spectra (Fig. S3). SEM images indicate that the PGE surface displays smooth and flake-like morphology of the graphite (Fig. 2A), whereas $CoSn(OH)_6$ homogeneously dispersed onto the PGE surface as nearly a cubic structure with particle size ranges between 0.23 and 0.76 µm (Fig. 2B). Unlike the bare PGE, the poly(BPB)@PGE surface exhibits a distinct morphological shift characterized by a uniform "haze", which serves as visual evidence of the successful deposition of the polymer as a continuous, thin-film layer (Fig. 2C). Moreover, when these materials are modified together onto the bare PGE surface (Fig. 2D and F), the polymer covers the $CoSn(OH)_6$/PGE surface in the form of a very thin film. Especially, this is clearly observable in the enlarged image of Fig. 2F (magnification: 100 nm×30000) and reflects almost both morphological properties that arise from both $CoSn(OH)_6$ and poly(BPB) materials.

EDX analysis was also employed to validate the existence of $CoSn(OH)_6$ and poly(BPB) on the PGE surface. The spectra of bare PGE revealed characteristic signals of the elements C (89.4%), O (8.2%), and Si (2.4%) (Fig. S3A), confirms the graphite and clay mineral content of PGE[23]. The characteristic signals of Co (7.0%) and Sn (6.1%) appeared after the modification of $CoSn(OH)_6$ onto PGE (Fig. S3B). Furthermore, electrodeposition of BPB onto the PGE surface also gives its distinctive signals of Br (0.3%) and S (0.1%) (Fig. S3C). These typical elements of Co (2.8%), Sn (1.7%), Br (0.2%) and S (0.1%) also emerge after the dual modification of $CoSn(OH)_6$ and poly(BPB) on the PGE surface (Fig. S3D). The mentioned elemental composition states a quantitative proof for the prospering integration of $CoSn(OH)_6$ and poly(BPB) on the PGE. In conclusion, all supporting evidences obtained from electrochemical and morphological characterization studies reflect the successful preparation of the poly(BPB)@$CoSn(OH)_6$/PGE.

The EDS mapping analysis was further performed for the rigorous confirmation of the structural architecture of the composite electrode (Fig. S4). The signals corresponding to Co, Sn, and O are localized predominantly within the cubic domains, validating the successful synthesis of the $CoSn(OH)_6$ inorganic phase. In contrast, the distinctive elements of the organic polymer—specifically Br and S—exhibit a pervasive, uniform intensity across the entire scanning area, regardless of the underlying inorganic cubic structures. This widespread elemental presence effectively confirms that the poly(BPB) layer acts as a continuous, thin-film blanket across the substrate rather than forming isolated clusters. Consequently, the contrast difference observed between the SEM micrograph of the proposed modified electrode and the bare PGE perfectly matches the homogeneous distribution of Br and S, revealing the architectural integrity of the poly(BPB)@$CoSn(OH)_6$/PGE interface.

## The examination of optimal conditions for the electrode fabrication step and the pH effect

The amounts of $CoSn(OH)_6$ and the poly(BPB) layer can have a direct influence on the cyclic voltammetric response of DPHN, because the enhanced thickness of modification material can decelerate the electron transfer due to a decrease in active sites on the electrode. In this conjunction, the immersion time of pencil leads into $CoSn(OH)_6$ suspension, BPB concentration, and cycle number during the electropolymerization process has been optimized. Figure S4A shows the CVs of 0.50 mM DPHN in pH 7.0 PBS recorded based on immersion times (30, 60, 90, 120, 180 s) of pencil leads into 2.0 mg $mL^{-1}$ $CoSn(OH)_6$ suspension at a stable BPB concentration of 0.30 mM, and the number of polymerization cycles of 3, respectively. The CV results are also given as $I_p$ (µA) versus immersion time (s) plots (Fig. S5B). The $I_p$ of DPHN gradually increased between 30 and 90 s and reached its highest level at 90 s. On the other hand, a distinct decline was observed after 90 s. Although the deposition step was carried out within a short immersion period, the $CoSn(OH)_6$ phase could still adhere effectively to the PGE surface. This behavior may be associated with the non-uniform surface texture of PGE, which contains graphite domains together with clay-based components. The rough and heterogeneous nature of this structure can create suitable regions for retaining $CoSn(OH)_6$ particles through physical attachment. Moreover, the hydroxyl-rich surface of $CoSn(OH)_6$ may interact with silicate/silanol-containing regions of the clay component, contributing to interfacial stabilization through hydrogen-bond-assisted contact. These factors support the formation of a sufficiently stable modifier layer on the electrode surface despite the short immersion duration. The decrease in $I_p$ indicates that the long immersion time, higher than 90 s, may cause a high loaded concentration of $CoSn(OH)_6$ and a decline in efficiency of the poly(BPB)@$CoSn(OH)_6$ composite. This is probably due to the limited mass transfer of DPHN to the PGE surface. Consequently, 90 s of immersion time displays an efficient balance for effective interaction between the poly(BPB) and $CoSn(OH)_6$ composite for DPHN sensing. The effect of the concentration of monomer BPB (Fig. S5C,D) and the cycle number (Fig. S5E,F) during the electropolymerization process was also investigated by the same procedure. The selectivity can be enhanced by electropolymerizing a homogeneously thick and stable poly(BPB) film, so the investigation of the suitable conditions for the monomer BPB number of cycles is mandatory for electrochemical sensing. The electrode surface reaches saturation in high concentrations and cycle number after 0.30 mM and 3, respectively. The highest level of $I_p$ was obtained for the conditions of 0.30 mM BPB and 3 cycles for these parameters. These values exhibit the highest binding efficiency of $CoSn(OH)_6$ to the poly(BPB) network. As a result, the optimum conditions for BPB concentration and cycle number were identified as 0.30 mM and 3 cycles, respectively.

The pH impact on the oxidation signal of DPHN was examined in B-RB with pH ranging from 4.0 to 11.0. As can be seen from Fig. 3A, the oxidation peak that appeared at + 1.10 V for pH 4.0 shifts to the cathodic region with the pH increment, confirming the proton involvement in the electrochemical oxidation process of DPHN[47]. Furthermore, the $I_p$ (µA) versus pH plots were illustrated in Fig. 3B. The $I_p$ comes up to its highest level at the pH of 10.0, and $I_p$ decreases at higher pH values, clarifying that the electro-activity of DPHN declines at more basic conditions than pH 10.0. This clarifies that the B-RB condition of pH 10.0, accompanied by the best voltammetric response to DPHN at poly(BPB)@$CoSn(OH)_6$/PGE.

The linear relationship between pH and peak potential ($E_p$) was expressed according to the equation of $E_p(V) = -0.0651 \times (pH) + 1.3842$ with a of $R^2 = 0.9977$ (Fig. 3C). The slope found from the plots (0.0651 V $pH^{-1}$)

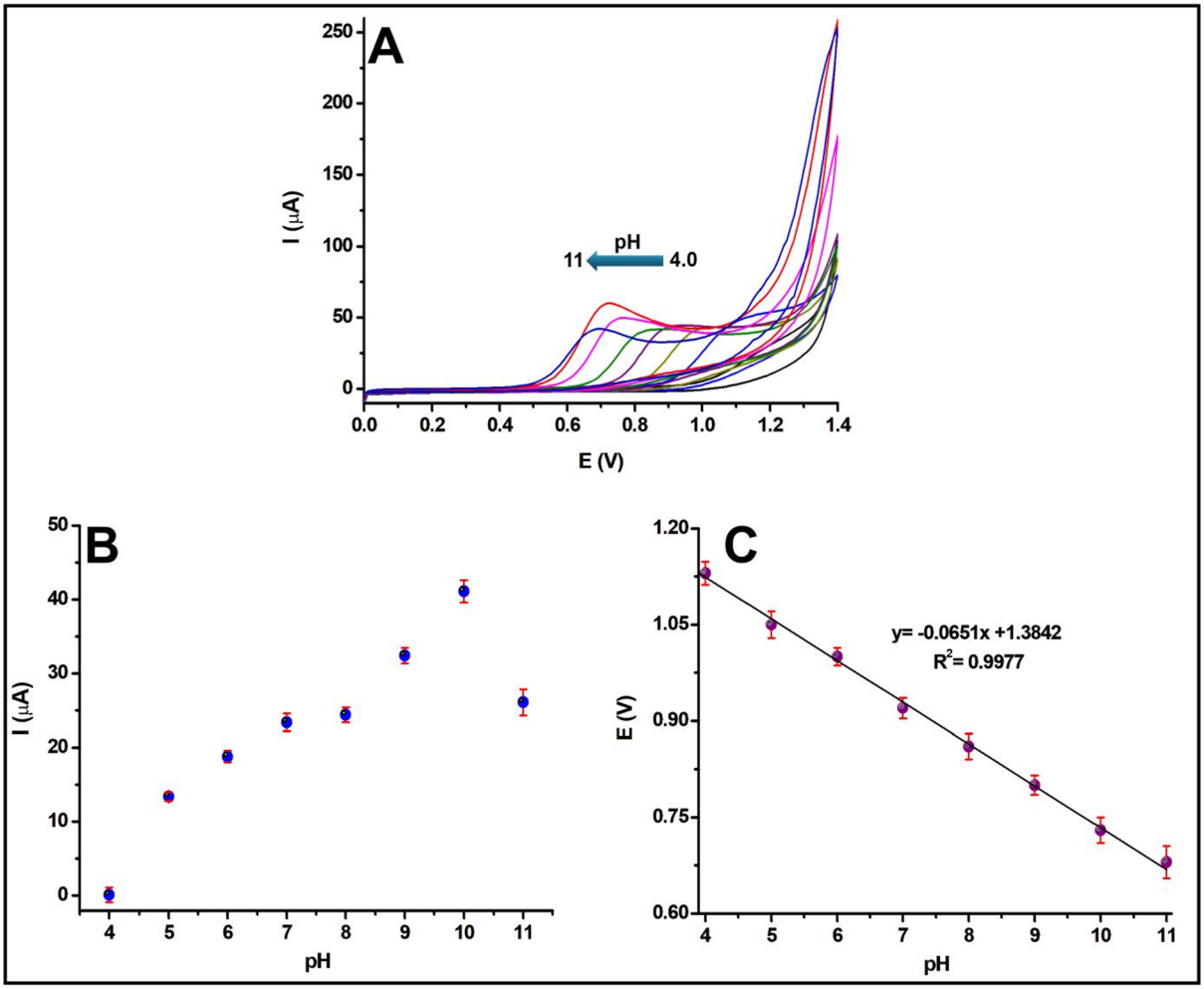



**Fig. 3**. (**A**) The CVs of DPHN (0.50 mM) in various pH conditions (4.0 - 11) of B-RB solution at poly(BPB)@$CoSn(OH)_6$/PGE (RAP: 0 - +1.40 V, $v = 50$ mV $s^{-1}$), (**B**) the dependence of $I_p$ versus pH, and (**C**) the plot of $E_p$ versus pH ($n = 3$).

is close to the theoretical Nernst value (0.0591) with a slight discrepancy, clarifying the equal numbers of $e^-$ and $H^+$ taking part in electrocatalytic oxidation of DPHN at poly(BPB)@$CoSn(OH)_6$/PGE[6].

## The sweep rate influence

The influence of sweep rate on the anodic peak of DPHN was also examined by recording the CVs of DPHN (0.50 mM) in the B-RB solution (pH = 10.0) for variable sweep rates (10 → 1000 mV $s^{-1}$) at poly(BPB)@$CoSn(OH)_6$/PGE (Fig. 4A). The $I_p$ goes linearly with the square root of the scan rate ($v^{1/2}$) stating with the equation of $I_p(\mu A) = 7.616 \times v^{1/2} - 17.1346$, with $R^2$ of 0.9985, which denotes that the electrooxidation current is limited by DPHN diffusion to the poly(BPB)@$CoSn(OH)_6$/PGE surface (Fig. 4B). This result was affirmed by the slope (0.5438) of the log $I_p$ versus log $v$ plot, which is nearly close to 0.5 (Fig. 4C) and reflects the characteristic of a diffusion-controlled process[47].

To clarify the micro-kinetic pathway and verify the charge stoichiometry of the process, the peak width at half-height (FWHM) was evaluated as an alternative diagnostic tool for the completely irreversible regime. At a moderate velocity of 50 mV $s^{-1}$, where the faradaic response is optimally decoupled from charging currents, the voltammetric profile exhibited a well-resolved morphology. Based on the graphical boundaries at half-peak height, the FWHM was extracted from the difference between the forward and backward potential coordinates (0.809–0.720 V), yielding a discrete value of 0.089 V. For processes governed by slow interfacial charge transfer, this broadness is fundamentally coupled to kinetic parameters through the formulation (2). Computing these boundary conditions for FWHM (0.089 V), molar gas constant ($R = 8.314$ J $K^{-1}$ $mol^{-1}$), temperature (T = 298.15 K), electron transfer coefficient for the anodic process (α), number of electron (n) and Faraday constant (F = 96485 C $mol^{-1}$), yields a combined α × n value of 1.017[48]. Typically, "α" is supposed to be 0.50 for an irreversible redox process on the electrode surface[49], the "n" participating in the oxidation of DPHN resolves to 2.03 close to 2.0, effectively authenticating the mechanistic pathways of DPHN through a rigorous, diffusion-compliant framework. This value is also in good agreement with the electro-oxidation mechanism of DPHN (Fig. S6) suggested by a published work[6].

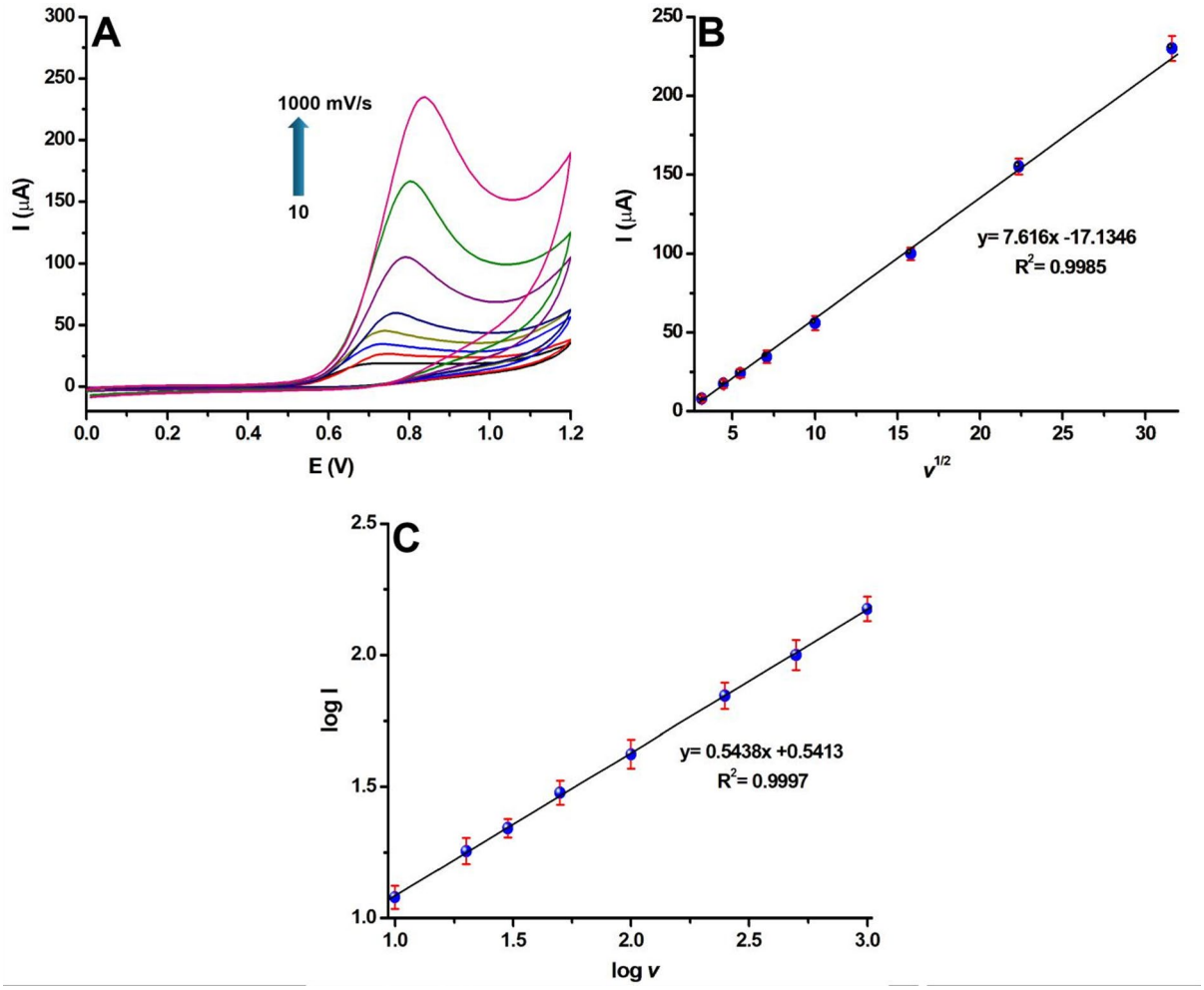



**Fig. 4**. (**A**) The CVs of DPHN (0.50 mM) in the B-RB solution (pH = 10.0) for variable sweep rates (10 → 1000 mV $s^{-1}$) at poly(BPB)@$CoSn(OH)_6$/PGE (RAP: 0 – +1.20 V), the dependences of (**B**) $I_p$ versus $v^{1/2}$, and (**C**) log $I_p$ versus log $v$ ($n = 3$).

$$FWHM = 3.53 \times \frac{RT}{\alpha\, nF} \tag{2}$$

## The cyclic voltammetric behavior of DPHN at poly(BPB)@$CoSn(OH)_6$/PGE

The electrochemical behavior of DPHN was examined by CV measurements recorded in B-RB solution (pH = 10.0), in the absence (0 mM) (Fig. 5A) and presence of 0.50 mM DPHN (Fig. 5B) at PGE (curve a), poly(BPB)@PGE (curve b), $CoSn(OH)_6$/PGE (curve c), and poly(BPB)@$CoSn(OH)_6$/PGE (curve d). As can be comprehended from the CVs, apart from negligible current increases at high potentials, no redox peaks were observed in the absence of DPHN at any of the electrodes (Fig. 5A). On the other hand, the electro-oxidation of DPHN shows itself as a distinct peak ($E_p$ = + 0.75 V and $I_p$ = 13.8 μA) at PGE (Fig. 5B, curve a). The $E_p$ was slightly shifted to + 0.73 V with a notable change in $I_p$ (23.8 μA) after the coating of poly(PBP) onto PGE (curve b). Furthermore, the oxidation peak was also observed at + 0.73 V with a nonignorable improvement in $I_p$ (19.7 μA) with the adsorption of $CoSn(OH)_6$ at PGE (curve c). The increased voltammetric responses obtained from single modifications of only one component of these materials, can be attributed to their good conductivity properties and large active surface areas, which facilitate the charge transfer between DPHN and PGE surface. In addition, the dual use of poly(BPB) and $CoSn(OH)_6$ on the PGE surface clearly demonstrates a synergistic advancement by showing a significant change in $I_p$ (41.1 μA) at + 0.72 V compared with poly(BPB)@PGE (curve b) and $CoSn(OH)_6$/PGE (curve c). The pronounced oxidation response obtained on the Poly(BPB)@$CoSn(OH)_6$/PGE electrode demonstrates a collaborative contribution of the poly(BPB) film and the $CoSn(OH)_6$ structure to the sensing mechanism. This increase can be explained by various interactions. One of them is the more dominant conductivity of the polymeric film, along with the π-π interaction and hydrogen bond formation between DPHN and poly(BPB), all of which lead to a significant increase in the signal. Secondly, the -OH groups in $CoSn(OH)_6$ provide strong hydrogen bonds between tertiary amine groups in DPHN, which also contribute to signal enhancement. In addition, the $CoSn(OH)_6$ phase likely accelerates electron transfer kinetics by providing catalytically active sites and increased electroactive surface area. Therefore, the combined contribution of

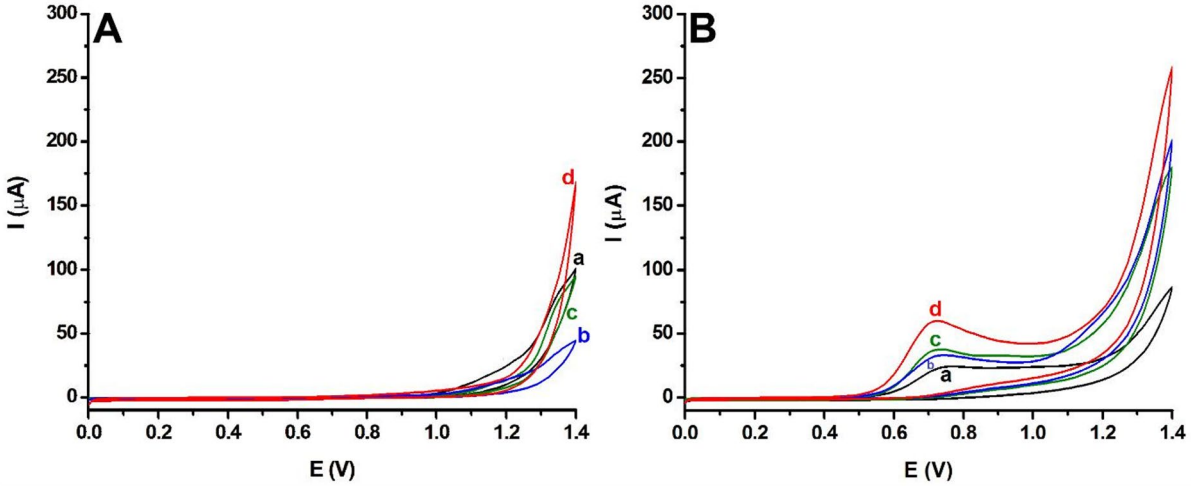



**Fig. 5**. The CVs of B-RB solution (pH = 10.0) (**A**) in the absence and (**B**) in the presence of DPHN (0.50 mM) at bare PGE (curve a), poly(BPB)@PGE (curve b), $CoSn(OH)_6$/PGE (curve c), and poly(BPB)@$CoSn(OH)_6$/PGE (curve d) (RAP: 0 – +1.40 V and $\nu = 50$ mV $s^{-1}$).

analyte deposition by poly(BPB) and the electrocatalytic activity of $CoSn(OH)_6$ leads to the improved sensing performance observed on the composite electrode. So, the $CoSn(OH)_6$ may have activated more electroactive poly(BPB) sites by promoting preferable interparticle contact and provided unique synergistic interactions between $CoSn(OH)_6$ and poly(BPB). The lower $R_{ct}$ value of poly(BPB)/$CoSn(OH)_6$/PGE in $Fe(CN)_6^{3-/4-}$ than that of the single component modified electrodes is considered to be evidence of a synergistic effect. In addition, the charge transfer kinetics at the modified interface was also evaluated quantitatively by calculating the charge transfer rate constant ($k^0$) in the Eq. (3)[50]:

$$k^0 = \frac{R \times T}{n^2 \times F^2 \times A_{Eff} \times C \times R_{ct}} \tag{3}$$

While all other parameters remain constant, the $k^0$ value changes inversely proportionally to $1/R_{ct}$. Therefore, the highest $k^0$ value being found in the proposed modified electrode, compared to bare PGE, and single component modified PGEs, confirms that the synergistic interaction between the polymer and the cubic structure effectively lowers the energy barrier for the electrochemical oxidation of DPHN. As a result of that, the composite modification (poly(BPB)@$CoSn(OH)_6$) may have improved the charge transfer at the PGE surface and displayed high voltammetric performance for the electro-oxidation of DPHN. Therefore, the fabrication of the DPHN sensor was designed through the poly(BPB)@$CoSn(OH)_6$/PGE.

## Determination of DPHN and analytical performance

Figure 6A illustrates the CVs achieved with consecutive addition of various concentrations of DPHN at poly(BPB)@$CoSn(OH)_6$/PGE under optimal conditions. The analytical calibration curve exhibited a rectilinear work range from 1.0 to 500.0 μM DPHN, and this linearity was identified with the equation of $I_p(\mu A) = 0.062 \times C_{DPHN}(\mu M) + 0.073$ ($R^2 = 0.9955$) (Fig. 6B). The LOD and quantification limit (LOQ) were calculated using the formulations of (3) and (4), respectively. The LOD and LOQ values were found to be 0.30 μM and 1.0 μM. Also, the electrode sensitivity was calculated based on Eq. (5) and calculated as 207 μA $mM^{-1}$ $cm^{-2}$).

$$LOD = 3 \times \frac{\text{standard deviation } (SD) \text{ of the measurable signal of lowest DPHN concentration}}{slope\ of\ calibration\ curve} \tag{4}$$

$$LOQ = 10 \times \frac{\text{SD of the measurable signal of lowest DPHN concentration}}{\text{slope of the calibration curve}} \tag{5}$$

$$Sensitivity = \frac{slope\ of\ the\ calibration\ curve}{A_{Eff}} \tag{6}$$

The obtained statistical data identifies the analytical performance of the fabricated DPHN sensor, and these results were compared with the performances of the prior reported DPHN sensors summarized in Table 1. As compiled in the table, a diverse range of analytical platforms—including screen-printed carbon electrode (SPCE), CPE, and GCE modified with various functional materials—have been successfully developed for DPHN quantification. This diversity demonstrates that electrochemical techniques are highly valued for antihistamine monitoring. However, CPE and GCE include time-consuming and inconvenient surface cleaning, polishing, and preparation steps for their reuses in electrochemical measurements, while PGE does not include these limitations. In addition,

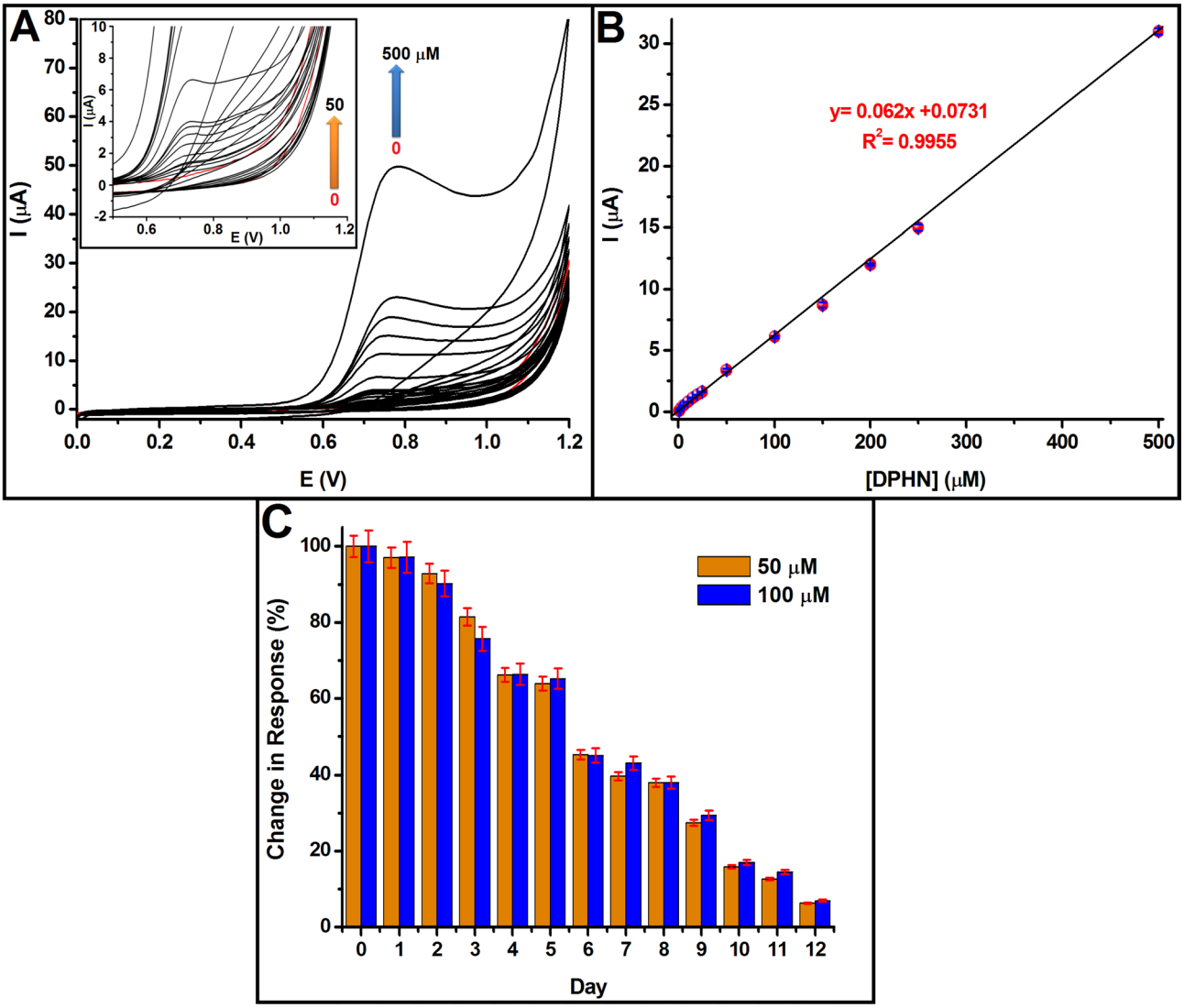



**Fig. 6**. (**A**) The CV response of various concentrations (0–500 μM) of DPHN at poly(BPB)@CoSn(OH)$_6$/PGE (RAP: 0 – +1.20 V and $\nu = 50$ mV s$^{-1}$), (**B**) the calibration plots for $I_p$ versus $C_{DPHN}$ ($I_p$ (μA) = 0.062×$C_{DPHN}$ (μM) + 0.073, $R^2$= 0.9955), and (**C**) the bar graphs for the inter-day responses of 50 μM and 100 μM DPHN at poly(BPB)@CoSn(OH)$_6$/PGE ($n = 3$).

SPCE, CPE, and GCE are overpriced compared to PGE. SPCE also has a disposable feature, but its surface cannot be regenerated as in PGE[23]. Furthermore, the recommended poly(BPB)@CoSn(OH)$_6$/PGE displays a lower LOD[13,14] and high applicability to a wider variety of real-world examples[5,6,13–15] for the determination of DPHN. Although pulse-based voltammetric techniques (such as DPV or SWV) often facilitate lower detection limits, the poly(BPB)@CoSn(OH)$_6$/PGE platform achieves a notable sensitivity (LOD = 0.30 μM). This value is highly competitive in a study used DPV at CuNPs/PAYR/GCE (LOD = 0.29 μM)[6]. Moreover proposed electrode has simultaneously maintaining structural simplicity and cost-efficiency. The comparative analysis confirms that our sensor offers a robust analytical response, bridging the gap between high-sensitivity requirements and the practical need for portable, low-cost electrochemical devices. A direct comparison of analytical figures of merit alone does not adequately reflect the practical value of an electrochemical sensing system. This developed multi-component architecture aims to achieve synergy beyond single modifications by combining the geometric advantages of CoSn(OH)$_6$ cubic structures with the electron transfer accelerating effect of the poly(BPB) matrix, rather than relying on a single active site. Importantly, the proposed system delivers a balanced analytical performance, combining a broad working range with consistent signal stability and successful implementation across chemically distinct real matrices. This highlights its suitability for practical analytical scenarios where reliability, ease of preparation, and cost-efficiency are often more critical than achieving ultra-trace detection limits under idealized conditions. From this perspective, the present work advances the field by shifting the focus from maximizing sensitivity alone toward developing realistically deployable electrochemical sensors with tangible application potential.

| Sensing platform | Electrochemically applied method | Working pH | Rectilinear work range (μM) | LOD (μM) | The applied real sample | Ref. |
|---|---|---|---|---|---|---|
| poly(BPB)@CoSn(OH)$_6$/PGE | CV | pH 10.0 B-RB | 1.0–500 | 0.30 | 1) Pharmaceutical cream formulation,<br>2) Artificial human blood serum<br>3) Natural spring water | This work |
| $Gd_2ZnMnO_6$/ZnO/Ionic liquid/CPE | DPV | pH 7.0 PBS | 0.09–70<br>90–900 | 0.033 | 1) Blood plasma<br>2) Human urine<br>3) Drug tablet | 3 |
| PVC/TpClPB/HP-β-CD/$Fe_3O_4$-NPs | Potentiometry | 3.5–7.0 PBS | 0.1–10,000 | 0.095 | 1) Milk<br>2) Human plasma | 5 |
| CuNPs/PAYR/GCE | DPV | pH 10.0 PBS | 1–3000 | 0.29 | 1) Drug tablet | 6 |
| SPCE | Potentiometry | 3.0–8.0 B-RB | 1.0–10,000 | 0.97 | 1) Pharmaceutical capsule | 13 |
| CPE | | 3.0–7.0 B-RB | | 0.98 | | |
| MCPE (DPH-TPB) | Potentiometry | 2.5–7.0 | 1.0–100,000 | 0.978 | 1) Pharmaceutical capsule | 14 |
| MSPCE (DPH-TPB) | | 2.5–8.0 | | 0.965 | | |
| ICPE | | 3.0–8.0 | | 0.976 | | |
| ISPCE | | 3.0–9.0 | | 0.968 | | |
| CdO/SWCNTs/[$C_4$mim]-[$PF_6$]/CPE | SWV | pH 8.5 PBS | 0.05–700 | 0.009 | 1) Pharmaceutical syrup<br>2) Pharmaceutical serum | 15 |
| $SrTiO_3$/N-GNS/GCE | AdsDPV | pH 7.0 PBS | 0.038–100 | 0.0021 | 1) Drug capsule<br>2) Blood serum<br>3) Urine | 16 |

**Table 1**. A comparison of analytical performance between the proposed and the prior published studies. HP-β-CD: 2-hydroxypropyl-β-cyclodextrin; TpClPB: Tetrakis(4-chlorophenyl) borate; PVC: Polivinyl chloride; PAYR: poly(Alizarin Yellow R); MCPE: DPH-tetraphenyl borate ion couple (DPH-TPB)/CPE; MSPCE: DPH-tetraphenyl borate ion couple (DPH-TPB)/SPCE; ICPE: Tricrysylphosphate (TCP)/CPE; ISPCE: DPH-tetraphenyl borate ion couple- tricrysylphosphate (Tricrysylphosphate, TCP)/SPCE; [C4mim]-[PF6]: 1-butyl-3-methylimidazolium hexafluoro phosphate; SWCNTs: Single wall carbon nanotubes; $SrTiO_3$/N-GNS: Nano cylindrical strontium titanate/N-doped graphene; FI-FFTCV: Flow Injection System by Fast Fourier Transform Continuous Cyclic Voltammetry; ABS: Acetate buffer solution.

The reproducibility, intra-day repeatability, and inter-day stability features of the poly(BPB)@CoSn(OH)$_6$/PGE were additionally examined under the optimal conditions. The reproducibility of fabricated poly(BPB)@CoSn(OH)$_6$/PGE was assessed at eight newly prepared composite electrodes by recording the CVs of 50 μM and 100 μM DPHN. The calculated relative standard deviation (RSD) values of 3.82% (for 50 μM) and 4.00% (for 100 μM) affirm that the parallels fabricated poly(BPB)@CoSn(OH)$_6$/PGEs display a remarkable reproducibility. Inter-day repeatability experiments were performed at a single electrode for at least 10 measurements with the same procedure, and the calculated RSD values of 3.32% (for 50 μM) and 4.26% (for 100 μM) prove the highly repeatable voltammetric responses at poly(BPB)@CoSn(OH)$_6$/PGE for DPHN determination. Thereafter, the intra-day stability feature of the composite electrode was also evaluated by monitoring the CV response of 50 μM and 100 μM DPHN over 10 days with the same experimental route at the same electrode (Fig. 6C). The developed sensor preserves its initial response for about 3 days. The poly(BPB)@CoSn(OH)$_6$/PGE notably loses its initial response by more than 10% on the 4th day, and the DPHN response gradually decreases on the following days. The electro-catalytic efficiency of poly(BPB)@CoSn(OH)$_6$/PGE to DPHN mostly disappeared on the last day (12th ). The huge drop after 12 days in the electrochemical response during the long-term stability study is mainly attributed to electrode fouling occurring on the poly(BPB)@CoSn(OH)$_6$/PGE surface during repeated experiments. In electrochemical processes, the generated oxidation products and/or reaction intermediates may have gradually adsorbed onto the active sites of the electrode surface, forming a partially insulating layer. This surface blockage may have hindered mass transfer and electron-transfer kinetics between DPHN and the electrode interface, thereby reducing the effective electroactive surface area and causing a progressive decrease in the anodic peak current response over time. Hence, the long-term usability of poly(BPB)@CoSn(OH)$_6$/PGE was investigated for 3 days in DPHN monitoring based on the tolerance limit of 10%. Although the system exhibits poor inter-day stability, this limitation is bypassed by utilizing the platform as a disposable or freshly prepared sensor. Because the modification phase requires less than 5.0 min and relies on low-cost substrates, long-term storage is unnecessary. Instead, generating a pristine electrode surface immediately prior to each analytical dynamic task completely circumvents surface deterioration. This straightforward, on-demand fabrication protocol offers a highly practical solution for robust, decentralized routine testing.

## Interference study and real samples analysis

To perform interference study, DPHN was further evaluated in the presence of some nitrogenous drugs (Ornidazole, Tinidazole, and Nitazoxanide), Chrysin drug, carbohydrates (Glucose and Sucrose), inorganic ions ($Na^+$, $Mg^{2+}$, $Ca^{2+}$, $Zn^{2+}$, $Fe^{3+}$, $NO_3^-$, and $SO_4^{2-}$), and biologically important molecules (glycine, ascorbic acid, uric acid, and urea) at between 1.0 and 100-fold molar concentration over DPHN. The evaluation was carried out based on the $I_p$ change (%) of poly(BPB)@CoSn(OH)$_6$/PGE in 50 μM DPHN for various potential interferences (Table S1), and the admissible tolerance in voltammetric response of ± 10% was taken into consideration. The

| | | Found with the standard addition-integrated CV method | | Found with UV–Vis reference method | |
|---|---|---|---|---|---|
| Sample | Added | Found | Recovery | Found | Recovery |
| Pharmaceutical lotion | 0 | 1.05% ±0.03 | 105.0% | 1.08% ±0.07 | 108.0% |
| | 0.5% | 1.45% ±0.06 | 96.7% | 1.49% ±0.05 | 99.3% |
| | 1.0% | 1.98% ±0.04 | 99.0% | 2.02% ±0.09 | 101% |

**Table 2**. The results of the determination of DPHN dosage in pharmaceutical lotion ($n = 3$).

| Sample | Spiked dosage (μM) | Found dosage (μM) | Recovery (%) for DPHN | RSD (%) |
|---|---|---|---|---|
| Tap water | 0 | 0 | – | – |
| | 25 | 26.6 | 106.3 | 1.88 |
| | 50 | 46.2 | 92.4 | 1.82 |
| Artificial human blood serum | 0 | 0 | – | – |
| | 25 | 24.5 | 98.0 | 1.10 |
| | 50 | 51.9 | 103.8 | 1.58 |

**Table 3**. The recovery results of DPHN dosage in tap water and artificial blood serum ($n = 3$).

interference effect of 100-fold $Na^+$, $Mg^{2+}$, $Ca^{2+}$, $Zn^{2+}$, $Fe^{3+}$, $NO_3^-$, $SO_4^{2-}$, Glucose, and Sucrose, 10-fold ascorbic acid, 1.0-fold Ornidazole, Tinidazole, Nitazoxanide, Chrysin, uric acid, urea, and glycine was found to be negligible and tolerable to the oxidation response of DPHN based on the tolerable ratio limit of 1:1. Thereby, the designed DPHN sensor mostly exhibits electrochemical inertness to other molecules. The results affirm the suitable selectivity of the poly(BPB)@CoSn(OH)$_6$/PGE for the DPHN determination.

The analytical performance of the proposed Standard Addition-Recovery coupled CV method was assessed for the quantification of DPHN in pharmaceutical lotion, with the UV-Vis spectrophotometric method serving as the reference. From the CV curves and standard addition calibration plots (Fig. S7) for non-spiked sample by CV method, the percentage amount of DPHN in the pharmaceutical lotion sample was calculated (Table 2). As can be understood from the table, the obtained results from CV (1.05% ±0.03) and UV-Vis methods (1.08% ±0.07) were found to be in convenience with the labeled value (1.0%) declared by the manufacturer and shows the successful feasibility and reliability of the proposed technique with sufficient accuracy and precision for the potential analysis of DPHN in pharmaceutical samples. A statistical comparison (Student's t-test and F-test) between the proposed method and a reference UV-Vis spectroscopic method[42] was utilized to validate the recommended DPHN sensing method (Table 2). The obtained experimental t values for both methods ($t_{CV}$ = 2.89 and $t_{UV-Vis}$= 2.77) were determined to be less than the critical t value of 4.30[17], which proved that the mean values of both methods do not show any notable difference; in other words, the accuracy of both methods is compatible. The calculated experimental F value (2.78) is less than the critical F value of 19.0[17], also indicating the inconsiderable difference between the standard deviations of these techniques. The spike-recovery experiments by CV, performed at 0.5% and 1.0% concentrations, yielded recovery rates of 96.7% and 99.0%, respectively (Table 2). These figures confirm that the method effectively minimizes matrix effect, which is often a significant challenge in the analysis of complex formulations such as lotions. When compared to the UV-Vis reference method, the proposed technique demonstrates excellent accuracy and reliability, offering a robust alternative for the quantification of DPHN in pharmaceutical matrices.

The advanced evaluation for the feasibility of the fabricated method was also examined by utilizing the DPHN recovery studies from tap water and artificial human blood serum samples. For this aim, the CVs of non-spiked and spiked (25 μM and 50 μM) DPHN samples were recorded under optimal conditions. Then, standard addition-integrated CV experiments were utilized by adding standards of DPHN, as in the pharmaceutical lotion. The results obtained for tap water and artificial human blood serum samples were given in Table 3. The recovery values between 92.4 and 106.3% reflect the high feasibility of the proposed sensing platform for the accurate and reliable determination of DPHN in complex matrices.

## Conclusion

This study represents an innovative voltammetric sensor performing a novel conductive polymer-supported metal hydroxyl-stannate-based composite, poly(BPB)@CoSn(OH)$_6$ modified PGE for the electrochemical detection of DPHN. The characterization techniques (such as EIS, SEM, EDX, XRD, and FT-IR) authenticate the successful preparation of the poly(BPB)@CoSn(OH)$_6$/PGE. The synergistic electrocatalytic features of poly(BPB)@CoSn(OH)$_6$ offer more electroactive sites and a high surface-to-volume ratio and improve the electrochemical performance for DPHN detection as compared to bare PGE. The CV experiments indicate that the poly(BPB)@CoSn(OH)$_6$/PGE displays a linear work range of 1.0–500.0 μM with a lower LOD value of 0.30 μM. The fabricated poly(BPB)@CoSn(OH)$_6$/PGE architecture demonstrated a favorable selectivity for DPHN tracking, maintaining its signal distribution within acceptable tolerances when cross-examined against the specific co-existing species and ions selected for the assays. The sensor exhibits remarkable applicability

in quantifying and identifying DPHN in pharmaceutical drug formulations, tap water, and artificial human blood serum with sufficient accuracy and precision. The proposed study underscores enormous potential for the fabricated poly(BPB)@$CoSn(OH)_6$ composite in electrochemical analysis of pharmaceutical, environmental, and biological samples, providing a scalable and versatile platform for advanced sensor evolution. In summary, the proposed composite can be integrated with other materials for the development of innovative composite structures, which will gain a place in their broad utilization of electrochemical sensor designs.

## Data availability

All data generated or analysed during this study are included in this published article.

Received: 31 March 2026; Accepted: 29 June 2026
Published online: 01 July 2026

## References

1. Norouzi, P., Ganjali, M. R., Nouryousefi, E., Shahtaheri, S. J. & Dinarvand, R. Trace detection of diphenhydramine by adsorption on a microelectrode at flow injection system by fast fourier transform continuous cyclic voltammetry. *Croat Chem. Acta*. **83**, 135–142 (2010).
2. Wolfson, A. R., Wong, D., Abrams, E. M., Waserman, S. & Sussman, G. L. Diphenhydramine: Time to move on? *J. Aller Cl. Imm-Pract*. **10**, 3124–3130 (2022).
3. Javad Tavakoli, M., Shabani-Nooshabadi, M. & Ziaie, N. Application of $Gd_2ZnMnO_6$/ZnO nanocomposite for electrochemical measurement of acetaminophen, diphenhydramine, and phenylephrine. *Anal. Chim. Acta*. **1279**, 341766 (2023).
4. Walker, A., Delle Donne, A., Douglas, E., Spicer, K. & Pluim, T. Novel use of dexmedetomidine for the treatment of anticholinergic toxidrome. *J. Med. Toxicol.* **10**, 406–410 (2014).
5. Marzouk, H. M., Ibrahim, E. A., Hegazy, M. A. & Saad, S. S. A reliable electrochemical sensor based on functionalized magnetite nanoparticles for over the counter allergy medication abuse sensing in biological fluids. *Electroanalysis* **34**, 552–560 (2022).
6. Amini, N. et al. Construction of a sensitive electrochemical sensor for diphenhydramine and 8-chlorotophylline as a dimenhydrinate drug based on copper nanoparticles and polyalizarin yellow at two applied potentials. *J. Appl. Electrochem*. **52**, 617–626 (2022).
7. Tipparat, P., Lapanantnoppakhun, S., Jakmunee, J. & Grudpan, K. Determination of diphenhydramine hydrochloride in some single tertiary alkylamine pharmaceutical preparations by flow injection spectrophotometry. *J. Pharm. Biomed. Anal.* **30**, 105–112 (2002).
8. Ulu, S. T. & Elmali, F. T. Spectrophotometric method for the determination, validation, spectroscopic and thermal analysis of diphenhydramine in pharmaceutical preparation. *Spectrochim Acta Mol. Biomol. Spectrosc.* **77**, 324–329 (2010).
9. Dönmez, Ö. A., Aşçı, B., Bozdoğan, A. & Sungur, S. Simultaneous determination of potassium guaiacolsulfonate, guaifenesin, diphenhydramine HCl and carbetapentane citrate in syrups by using HPLC-DAD coupled with partial least squares multivariate calibration. *Talanta* **83**, 1601–1605 (2011).
10. Ye, L. & Stewart, J. T. HPLC determination of an ondan-setron and diphenhydramine mixture in 0.9% Sodium chloride injection. *J. Liq Chromatogr. Relat. Technol.* **19**, 711–718 (1996).
11. Basavaiah, K. & Charan, V. S. Titrimetric and spectrophotometric assay of some antihistamines through the determination of the chloride of their hydrochlorides. *Il Farmaco*. **57**, 9–17 (2002).
12. Miao, C. et al. An ultrasensitive electrochemiluminescence sensor for detecting diphenhydramine hydrochloride based on l-cysteine-functionalized multiwalled carbon nanotubes/gold nanoparticles nanocomposites. *Sens. Actuators B Chem.* **213**, 5–11 (2015).
13. Frag, E. Y., Mohamed, G. G. & El-Sayed, W. G. Potentiometric determination of antihistaminic diphenhydramine hydrochloride in pharmaceutical preparations and biological fluids using screen-printed electrode. *Bioelectrochemistry* **82**, 79–86 (2011).
14. Akl, M. A., Frag, E. Y., Mohamed, G. G. & Bashanaini, M. S. Construction of modified screen-printed and carbon paste electrodes for electrochemical determination of antihistaminic diphenhydramine hydrochloride in pure and pharmaceutical preparations. *Int. J. Electrochem. Sci.* **8**, 11546–11563 (2013).
15. Cheraghi, S. & Taher, M. A. Fabrication of CdO/single wall carbon nanotubes modified ionic liquids carbon paste electrode as a high performance sensor in diphenhydramine analysis. *J. Mol. Liq.* **219**, 1023–1029 (2016).
16. Punde, N. S., Rajpurohit, A. S. & Srivastava, A. K. Sensitive electrochemical platform based on nano-cylindrical strontium titanate/N-doped graphene hybrid composite for simultaneous detection of diphenhydramine and bromhexine. *Electrochim. Acta*. **319**, 727–739 (2019).
17. Karakaya, S., Demir, C., Zaman, B. T., Bakırdere, S. & Dilgin, Y. Conductive poly (bromophenol red) film coated graphene oxide-ZnO nanocomposite modified electrode for enzymeless voltammetric determination of ethyl-paraoxon. *J. Food Compos. Anal.* **141**, 107393 (2025).
18. Rosie, N. T., Chelfi, T., Hach, B., Massai, H. B. B. & Laural N. C. Immobilization of organic compounds on an modified electrode: The electrochemical sensor route. *Bullet Catal. Soc. Ind.* **9**, 68–73 (2010).
19. Fatibello-Filho, O., Dockal, E. R., Marcolino-Junior, L. H. & Teixeira, M. F. Electrochemical modified electrodes based on metal-salen complexes. *Anal. Lett.* **40**, 1825–1852 (2007).
20. Atta, N. F., Galal, A. & Azab, S. M. Gold nanoparticles modified electrode for the determination of an antihypertensive drug. *Electroanalysis* **24**, 1431–1440 (2012).
21. Mani, V., Vilian, A. E. & Chen, S. M. Graphene oxide dispersed carbon nanotube and iron phthalocyanine composite modified electrode for the electrocatalytic determination of hydrazine. *Int. J. Electrochem. Sci.* **7**, 12774–12785 (2012).
22. Amini, N., Shamsipur, M., Gholivand, M. B. & Barati, A. A glassy carbon electrode modified with carbon quantum dots and polyalizarin yellow R dyes for enhanced electrocatalytic oxidation and nanomolar detection of L-cysteine. *Microchem J.* **131**, 9–14 (2017).
23. Dilgin, D. G., Vural, K., Karakaya, S. & Dilgin, Y. Simple, sensitive, and cost-effective voltammetric determination of salbutamol at a pencil graphite electrode modified with Nafion and functionalized multi-walled carbon nanotubes. *Monatsh Chem.* **155**, 143–153 (2024).
24. Mutharani, B., Ranganathan, P. & Chen, S. M. Chitosan-gold collapse gel/poly (bromophenol blue) redox-active film. A perspective for selective electrochemical sensing of flutamide. *Int. J. Biol. Macromol.* **124**, 759–770 (2019).
25. Sivasankaran, U., Thomas, A., Jose, A. R. & Kumar, K. G. Poly (bromophenol blue)-gold nanoparticle composite: An efficient electrochemical sensing platform for uric acid. *J. Electrochem. Soc.* **164**, B292–B297 (2017).
26. Khoshfetrat, S. M. & Chegeni, I. Rational design of $Ti_3C_2$ MXene nanocomposite with bromophenol blue for efficient signal amplification: Sensitive electrochemical detection of cardiac troponin I in patient plasma. *Sens. Actuators B Chem.* **397**, 134668 (2023).
27. Subbarayan, S., Natesan, M. & Chen, S. M. Simple synthesis of $CoSn(OH)_6$ nanocubes for the rapid electrochemical determination of rutin in the presence of quercetin and acetaminophen. *New. J. Chem.* **44**, 11271–11281 (2022).

28. Wang, Z., Wang, Z., Wu, H. & Lou, X. W. Mesoporous single-crystal $CoSn(OH)_6$ hollow structures with multilevel interiors. *Sci. Rep.* **3**, 1391 (2013).
29. Luo, B., Xu, S., Yan, X. & Xue, Q. Graphene nanosheets supported hollow Pt&$CoSn(OH)_6$ nanospheres as a catalyst for methanol electro-oxidation. *J. Power Sources*. **205**, 239–243 (2012).
30. Cheng, P., Ni, Y., Yuan, K. & Hong, J. Fast sonochemical synthesis of $CoSn(OH)_6$ nanocubes, conversion towards shape-preserved $SnO_2$–$Co_3O_4$ hybrids and their photodegradation properties. *Mater. Lett.* **90**, 19–22 (2013).
31. Zhang, W. J. A review of the electrochemical performance of alloy anodes for lithium-ion batteries. *J. Power Sources*. **196**, 13–24 (2011).
32. Raj, B. G. S., Wu, J. J., Asiri, A. M. & Anandan, S. Hybrid $SnO_2$–$Co_3O_4$ nanocubes prepared via a $CoSn(OH)_6$ intermediate through a sonochemical route for energy storage applications. *RSC Adv.* **6**, 33361–33368 (2016).
33. Aruchamy, G. & Thangavelu, S. Bifunctional CoSn $(OH)_6$/$MnO_2$ composite for solid-state asymmetric high power density supercapacitor and for an enhanced OER. *Electrochim. Acta*. **344**, 136141 (2020).
34. Satpathy, B. K., Raj, C. R. & Pradhan, D. Facile room temperature synthesis of CoSn $(OH)_6$/g-$C_3N_4$ nanocomposite for oxygen evolution reaction. *Electrochim. Acta*. **433**, 141250 (2022).
35. Guo, W., Li, X., Gao, X., Zeng, W. & Wang, X. Designed synthesis of Fe-doped $CoSn(OH)_6$ nanocubes with enhanced N-butyl alcohol gas sensing properties. *Sens. Actuators B Chem.* **379**, 133292 (2023).
36. Lin, X. et al. Photocatalytic $CO_2$ reduction promoted by uniform perovskite hydroxide $CoSn(OH)_6$ nanocubes. *Appl. Catal. B: Environ.* **224**, 1009–1016 (2018).
37. Sangili, A. et al. Highly selective voltammetric sensor for l-tryptophan using composite-modified electrode composed of $CuSn(OH)_6$ microsphere decorated on reduced graphene oxide. *J. Phys. Chem. C.* **124**, 25821–25834 (2020).
38. Qin, Y. et al. An electrochemical biosensor of Sn@C derived from $ZnSn(OH)_6$ for sensitive determination of acetaminophen. *Microchem J.* **175**, 107128 (2022).
39. Shu, Y. et al. Cube-like CoSn $(OH)_6$ nanostructure for sensitive electrochemical detection of $H_2O_2$ in human serum sample. *Sens. Actuators B Chem.* **241**, 528–533 (2017).
40. Şaylan, M. et al. Synthesis of nanocube-shaped cobalt tin hydroxides for the preconcentration of lead in environmental seawater collected from Antarctic region. *ChemistrySelect* **9**, e202304110 (2024).
41. Karakaya, S. & Dilgin, Y. The application of multi-walled carbon nanotubes modified pencil graphite electrode for voltammetric determination of favipiravir used in COVID-19 treatment. *Monatsh Chem.* **154**, 729–739 (2023).
42. Al Bratty, M. Visible spectrophotometric determination of chlorpheniramine maleate and diphenhydramine hydrochloride in raw and dosage form using potassium permanganate. *Orient. J. Chem.* **32**, 885–894 (2016).
43. Wang, J. F. et al. Boosting lithium storage performance of Co-Sn double hydroxide nanocubes in-situ grown in mesoporous hollow carbon nanospheres. *Electrochim. Acta*. **465**, 142971 (2023).
44. Jamil, S., Ahmad, H., Khan, S. R. & Janjua, M. R. S. A. First synthetic study of cube-like cobalt hydroxystannate nanoparticles as photocatalyst for Drimarene red K-4BL degradation and fuel additive. *J. Clust Sci.* **29**, 685–696 (2018).
45. Li, B., Zhang, G. X., Huang, K. S., Qiao, L. F. & Pang, H. One-step synthesis of $CoSn(OH)_6$ nanocubes for high-performance all solid-state flexible supercapacitors. *Rare Met.* **36**, 457–464 (2017).
46. Yang, G. J. et al. Characterization, growth mechanism and application of network poly (bromophenol blue). *J. Electroanal. Chem.* **604**, 48–56 (2007).
47. Buleandră, M. et al. Electrochemical study and determination of homovanillic acid, the final metabolite of dopamine, using an unmodified disposable electrode. *Molecules* **30**, 369 (2025).
48. Bard, A. J., Faulkner, L. R. & White, H. S. *Electrochemical Methods: Fundamentals and Applications* 2nd edn (Wiley, 2022).
49. Lee, T. W. et al. Realizing highly sensitive electrochemical determination of 2, 4, 6-trichlorophenol by tailoring the electronic state of a palladium–carbon cocatalyst. *Microchim Acta*. **192**, 454 (2025).
50. Lazanas, A. C. & Prodromidis, M. I. Electrochemical impedance spectroscopy a tutorial. *ACS Meas. Sci. Au*. **3**, 162–193 (2023).


## Acknowledgements

The authors thank the Scientific and Technological Research Council of Türkiye (TÜBİTAK, Project number: 124Z823) for the financial support provided for this study.

## Author contributions

Serkan Karakaya: Conceptualization, Investigation, Methodology, Software, Validation, Visualization, Writing – original draft, Writing – review and editing. Sezgin Bakırdere: Methodology, Writing – review and editing, Supervision. Meltem Şaylan: Methodology. Yusuf Dilgin: Methodology, Supervision, Writing – review and editing.

## Funding

This work was financially supported by the Scientific and Technological Research Council of Türkiye (TÜBİTAK) under Project No: 124Z823.

## Declarations

## Competing interests

The authors declare no competing interests.

## Statement

No AI tools were used for writing, editing, language refinement, or content generation in this manuscript.

## Additional information

**Supplementary Information** The online version contains supplementary material available at https://doi.org/10.1038/s41598-026-60620-9.

**Correspondence** and requests for materials should be addressed to S.K.

**Reprints and permissions information** is available at www.nature.com/reprints.

**Publisher's note** Springer Nature remains neutral with regard to jurisdictional claims in published maps and institutional affiliations.

**Open Access** This article is licensed under a Creative Commons Attribution-NonCommercial-NoDerivatives 4.0 International License, which permits any non-commercial use, sharing, distribution and reproduction in any medium or format, as long as you give appropriate credit to the original author(s) and the source, provide a link to the Creative Commons licence, and indicate if you modified the licensed material. You do not have permission under this licence to share adapted material derived from this article or parts of it. The images or other third party material in this article are included in the article's Creative Commons licence, unless indicated otherwise in a credit line to the material. If material is not included in the article's Creative Commons licence and your intended use is not permitted by statutory regulation or exceeds the permitted use, you will need to obtain permission directly from the copyright holder. To view a copy of this licence, visit http://creativecommons.org/licenses/by-nc-nd/4.0/.

© The Author(s) 2026